iScience

CellPress
OPEN ACCESS

Article

pSNAP: Proteome-wide analysis of elongating nascent polypeptide chains

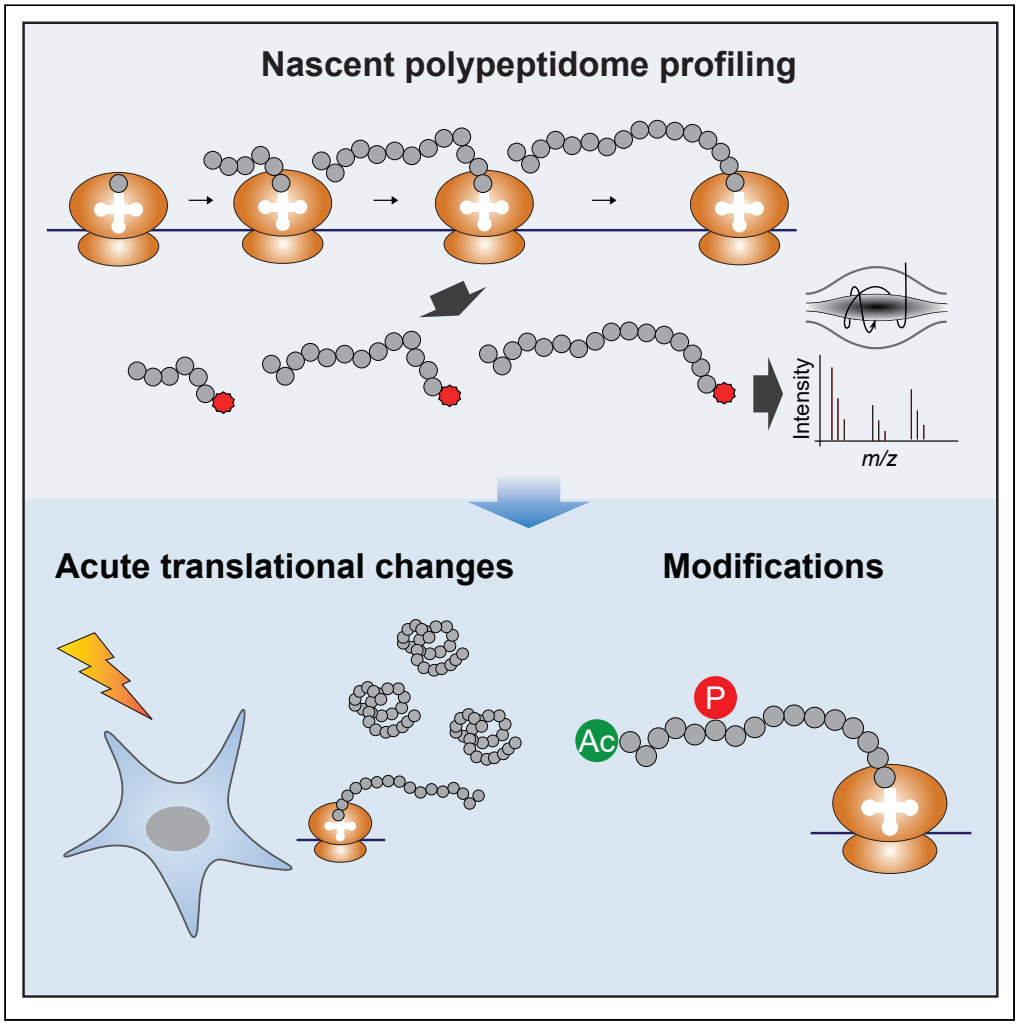

Junki Uchiyama, Rohini Roy, Dan Ohtan Wang, ..., Yuichiro Mishima, Yasushi Ishihama, Koshi Imami

yishiham@pharm.kyoto-u.ac.jp (Y.I.)
koshi.imami@riken.jp (K.I.)

Highlights

Nascent polypeptidome analysis with a simplified protocol

Quantification of acute changes in nascent polypeptides induced by external stimuli

Profiling and characterization of chemical modifications on nascent polypeptides

Uchiyama et al., iScience 25, 104516
July 15, 2022
https://doi.org/10.1016/j.isci.2022.104516

iScience

CellPress
OPEN ACCESS

Article

pSNAP: Proteome-wide analysis of elongating nascent polypeptide chains

Junki Uchiyama,[1] Rohini Roy,[2,3,4] Dan Ohtan Wang,[2,3,4,5] Kazuya Morikawa,[1] Yuka Kawahara,[6] Mio Iwasaki,[6] Chiaki Yoshino,[1] Yuichiro Mishima,[7] Yasushi Ishihama,[1,8,*] and Koshi Imami[1,9,10,11,*]

SUMMARY

Cellular global translation is often measured using ribosome profiling or quantitative mass spectrometry, but these methods do not provide direct information at the level of elongating nascent polypeptide chains (NPCs) and associated co-translational events. Here, we describe pSNAP, a method for proteome-wide profiling of NPCs by affinity enrichment of puromycin- and stable isotope-labeled polypeptides. pSNAP does not require ribosome purification and/or chemical labeling, and captures *bona fide* NPCs that characteristically exhibit protein N-terminus-biased positions. We applied pSNAP to evaluate the effect of silmitasertib, a potential molecular therapy for cancer, and revealed acute translational repression through casein kinase II and mTOR pathways. We also characterized modifications on NPCs and demonstrated that the combination of different types of modifications, such as acetylation and phosphorylation in the N-terminal region of histone H1.5, can modulate interactions with ribosome-associated factors. Thus, pSNAP provides a framework for dissecting co-translational regulations on a proteome-wide scale.

INTRODUCTION

Co-translational regulation, such as modifications of nascent polypeptide chains (NPCs) during translation, drives many aspects of cellular proteostasis, including protein folding, processing, subcellular targeting, and translational control (Aviner et al., 2021; Collart and Weiss, 2020; Schwarz and Beck, 2019). Therefore, monitoring co-translational events at the NPC level is crucial for understanding cellular proteome dynamics at the moment a peptide is born.

Current approaches for systematically profiling the newly synthesized proteome are mainly based on the capture of proteins metabolically labeled with stable isotope-labeled (SILAC) amino acids (Doherty et al., 2009; Klann et al., 2020; Schwanhäusser et al., 2009) or bioorthogonal amino acids such as azidohomoalanine (Dieterich et al., 2006; Eichelbaum et al., 2012; McShane et al., 2016). These methods allow us to profile mainly fully translated products (Eichelbaum et al., 2012; McShane et al., 2016), but cannot enrich NPCs actively being elongated by ribosomes in action. In contrast, puromycin is an aminoacylated tRNA analog that can be incorporated at the C-termini of elongating NPCs (Aviner, 2020). Hence, puromycin labeling has been extensively used to monitor protein synthesis in many applications, including imaging and immunoblotting, and in various systems ranging from cell-free translation to cultured cells and whole animals (Aviner, 2020). However, the utility of puromycin or its derivatives for proteome-wide analysis of NPCs has been limited due to the need for complicated procedures, including ribosome purification by ultracentrifugation (Aviner et al., 2013) and/or chemical labeling (Forester et al., 2018; Huang et al., 2021; Tong et al., 2020; Uchiyama et al., 2020) prior to affinity purification of NPCs. Furthermore, reliable detection of NPCs is often hampered by non-specific binding of high-background pre-existing proteins to beads or resin during affinity purification (Eichelbaum et al., 2012; Howden et al., 2013; Mellacheruvu et al., 2013).

To overcome these limitations, we have developed a method that combines quantitative proteomics and dual-pulse labeling with puromycin and SILAC amino acids, termed puromycin- and SILAC labeling-based nascent polypeptidome profiling (pSNAP). We demonstrate the broad utility of the method by applying it to both HeLa cells and primary cells to characterize rapid translational changes as well as modifications on NPCs such as protein N-terminal acetylation.

[1]Graduate School of Pharmaceutical Sciences, Kyoto University, Kyoto 606-8501, Japan

[2]Institute for Integrated Cell-Material Sciences (iCeMS), Kyoto University, Kyoto, 606-8501, Japan

[3]Center for Biosystems Dynamics Research, RIKEN, Kobe, Hyogo 650-0047, Japan

[4]Graduate School of Biostudies, Kyoto University, Kyoto 606-8501, Japan

[5]Wuya College of Innovation, Shenyang Pharmaceutical University, Shenyang 110001, China

[6]Department of Life Science Frontiers, Center for iPS Cell Research and Application, Kyoto University, Kyoto 606-8507, Japan

[7]Faculty of Life Sciences, Kyoto Sangyo University, Kita-ku, Kyoto 603-8555, Japan

[8]Laboratory of Clinical and Analytical Chemistry, National Institute of Biomedical Innovation, Health and Nutrition, Ibaraki, Osaka 567-0085, Japan

[9]PRESTO, Japan Science and Technology Agency (JST), Chiyoda-ku, Tokyo 102-0075, Japan

[10]RIKEN Center for Integrative Medical Sciences, Tsurumi-ku, Yokohama, Kanagawa 230-0045, Japan

[11]Lead contact

*Correspondence: yishiham@pharm.kyoto-u.ac.jp (Y.I.), koshi.imami@riken.jp (K.I.)

https://doi.org/10.1016/j.isci.2022.104516

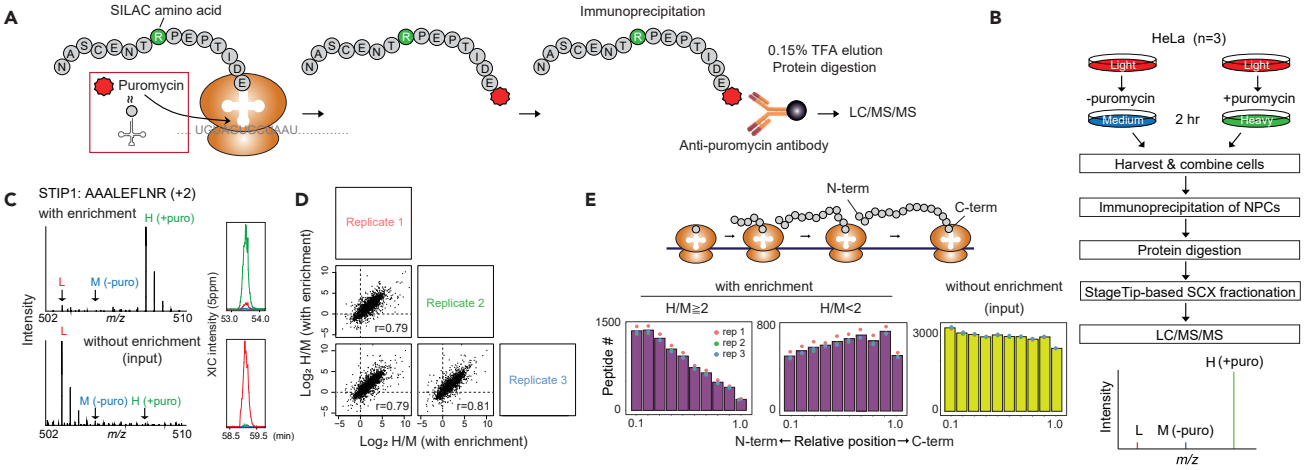

Figure 1. Profiling nascent polypeptide chains by pSNAP

(A) Principle of the enrichment of NPCs with the pSNAP.

(B) Schematic representation of pSNAP workflow. HeLa cells are pulse labeled for 2 h with a combination of 10 μM puromycin and heavy amino acids or with only medium-heavy amino acids. After IP of NPCs with anti-puromycin antibodies, NPCs are eluted with 0.15% TFA and digested into tryptic peptides. The resulting peptide sample is fractionated into 7 fractions using an SCX StageTip (see STAR Methods) and each fraction is analyzed by LC/MS/MS. Heavy-to-medium (H/M) ratios represent the degree of enrichment of NPCs.

(C) Exemplary MS spectra for AAALEFLNR (STIP1) obtained with (top) and without (bottom) enrichment. The isotope clusters of the L, M, and H peaks correspond to non-specific proteins from the pre-existing proteome pool and from the "medium"-labeled proteins and "heavy"-labeled NPCs, respectively. Extracted ion chromatograms (XICs) of monoisotopic peaks of the L, M and H peptides are shown.

(D) Multi-scatter plots of $\log_2$ H/M ratios from three independent experiments of pSNAP.

(E) pSNAP can enrich NPCs. (top) The ribosome elongates an NPC from its N-terminal end to the C-terminal end. Thus, positions of NPC-derived tryptic peptides are biased toward the N-termini of proteins. (bottom) Relative starting positions of identified peptides within proteins. The bars represent averaged values from three independent experiments.

RESULTS AND DISCUSSION

pSNAP enables global profiling of nascent polypeptide chains

We reasoned that NPCs incorporating puromycin could be immunoprecipitated with an anti-puromycin antibody (Figure 1A), thereby allowing for proteome-wide analysis of NPCs by means of liquid chromatography-tandem mass spectrometry (LC/MS/MS). We first confirmed that puromycin incorporation into proteins was translation-dependent (Figure S1A) and that no marked degradation of the puromycin-labeled proteins occurred during 2 h treatment of HeLa cells with 10 μM puromycin (Figure S1B). We chose 10 μM puromycin because this concentration could label a wide range of NPCs, while higher concentrations (>30 μM) of puromycin resulted in the production of smaller NPCs (Figure S1C). This is consistent with the fact that puromycin binds to NPCs in competition with aminoacyl-tRNAs, and therefore puromycin at very low concentration (0.04 μM) can bind only to full-length NPCs at the C-terminus (Miyamoto-Sato et al., 2000). We then tested a monoclonal antibody against puromycin (clone 12D10) and found that puromycylated proteins could be effectively immunoprecipitated when appropriate amounts of the antibody and input protein were used (Figure S1D). Based on these results, we used 15 μg antibodies per 250 μg protein input for subsequent immunoprecipitation (IP) experiments.

We next sought to profile individual NPCs with LC/MS/MS. For proof of concept, HeLa cells were pulse-labeled with a combination of puromycin and "heavy (H)" amino acids (Arg'10' and Lys'8') for 2 h (Figure 1B). As a control, cells were treated with only "medium-heavy (M)" amino acids (Arg'4' and Lys'4') and puromycin was omitted. The use of "M" and "H" labeling enabled us to distinguish *bona fide* NPCs (H-labeled) from non-specific proteins [light (L)- or M-labeled]. As expected, H-labeled proteins were highly enriched in the IP sample (Figure 1C top) while pre-existing proteins were predominantly observed in the input (Figure 1C bottom). Overall, we observed high H/M ratios (≧2) for 70% of 2,619 quantified proteins with good reproducibility (Figures 1D, S1E and Table S1), demonstrating that pSNAP can profile thousands of NPCs. In contrast, we observed low H/L ratios (<1) for 62% of the quantified proteins (Figure S1F) due to the high background resulting from non-specific binding of pre-existing proteins (L) to beads. These results highlight the importance of pulse labeling with SILAC amino acids to differentiate NPCs and pre-existing proteins.

Proteins captured by pSNAP exhibit a signature of elongating nascent polypeptides

Ribosomes elongate NPCs from their amino (N-) terminal end to their carboxy (C-) terminal end (Figure 1E top). In line with this directionality, the mapped positions of peptides with H/M≧2 clearly showed a bias toward the N-termini of the corresponding proteins (Figure 1E bottom), further supporting the enrichment of elongating NPCs. Notably, such a trend was not observed for less enriched peptides (i.e., H/M < 2) or input cell lysates (Figure 1E bottom).

To further evaluate pSNAP, we compared it with two orthogonal approaches, pSILAC (Schwanhäusser et al., 2009) and ribo-seq (Ingolia et al., 2009), used for studying protein synthesis at the levels of protein and mRNA, respectively. To this end, we used our input data (Figure 1E) as a 2 h pSILAC experiment and a publicly available ribo-seq dataset for HeLa cells (Stumpf et al., 2013). We found moderate correlations with the two independent methods; r = 0.49 (vs. pSILAC) and r = 0.40 (vs. ribo-seq) (Figure S1G); similar levels of correlation were also seen in a previous study using a biotin-puromycin-based approach (Aviner et al. Gene. Dev. 2014). These results indicate that pSNAP can accurately quantify translation products.

pSNAP with short pulse labeling enables quantitative profiling of nascent proteome

We next assessed the effect of pulse-labeling time on NPC capture. Previous studies using O-propargyl-puromycin (OPP) (Forester et al., 2018; Uchiyama et al., 2020) employed 2 h labeling, while a more recent study (Tong et al., 2020) performed only 15 min labeling. However, the trend of protein N-terminus-biased positions was not seen in the 15 min labeling method, in contrast to our results (Figure 1E bottom left), implying that NPCs cannot be sufficiently captured with such a short labeling time, or are hidden by non-specific binding of pre-existing proteins. Based on these prior experiments and the immunoblotting results (Figure S1B left panel), we chose 30 min as the shortest effective labeling time and used increased protein inputs (250, 500, and 750 μg) for pSNAP experiments. We found that this labeling time enabled us to profile NPCs. We observed high H/M ratios (Figure S2A, Table S2) and protein N-terminus-biased positions (Figure S2B), as seen in the case of 2 h labeling (Figure 1E left panel), though slightly fewer NPCs were quantified in the short labeling method compared to 2 h labeling (Table S2).

To further demonstrate the validity of the 30 min labeling method, we analyzed lipopolysaccharide (LPS)-induced translational responses with different periods of pulse labeling (30 min, 1 h, and 2 h). RAW264.7 macrophages were first treated with 100 ng/mL LPS for 1 h, and then switched to a medium containing puromycin and heavy amino acids. As a control, cells were treated with vehicle (water), and pulse-labeled with puromycin and medium-heavy amino acids. We successfully quantified NPCs including known LPS-regulated genes (e.g., Cxcl2, Junb, Rela, and Nfkbiz) regardless of the pulse-labeling time (Figures S2C, S2E and Table S2). These results established that even a labeling time as short as 30 min can be used to robustly detect translational responses using the pSNAP approach. It should be noted that we used a 2 h labeling time for the following experiments because it did not significantly affect cell viability (Figure S2D) or quantitative analysis (Figure S2C) and yielded sufficient amount of puromycylated NPCs (Table S2).

pSNAP allows quantitative nascent proteome profiling in primary neuronal cultures

In addition to HeLa cells, we applied pSNAP to mouse primary cortical neuron cultures, which contain a mixture of brain cell types but are highly enriched for neurons (Figure 2E). pSNAP revealed strong enrichment of peptides near the N-termini of proteins (Figure 2A–2C), and achieved highly sensitive detection of NPCs, including neuronal markers; NCAM1, FOXG1, and DCX (Table S3), supporting the validity of NPCs detection using pSNAP. We also quantified the differential NPC profiles between 5 and 14 days *in vitro* (DIV), and identified 122 and 203 significantly upregulated proteins in DIV5 and DIV14, respectively. (Figure 2D–2F and Table S3). These results overall reflect the known proteome dynamics during neuronal development *in vitro* (Frese et al., 2017). For example, nascent proteins related to "synaptic vesicle cycle" were overrepresented in DIV14 (Figure 2G), consistent with the occurrence of synapse formation and maintenance after development. In addition, both immunostaining and pSNAP confirmed that a presynaptic marker synaptophysin (SYPH) was upregulated in DIV14 (Figure 2E). Collectively, these results indicate that pSNAP captures genuine dynamics of NPCs in primary cultures and enables quantitative nascent proteome analysis.

Quantifying translational responses induced by a kinase inhibition

The ability to capture and quantify NPCs proteome-wide with high accuracy enables quantitative measurements of acute translational changes that allow cells to respond to specific stimuli. To illustrate this, we next

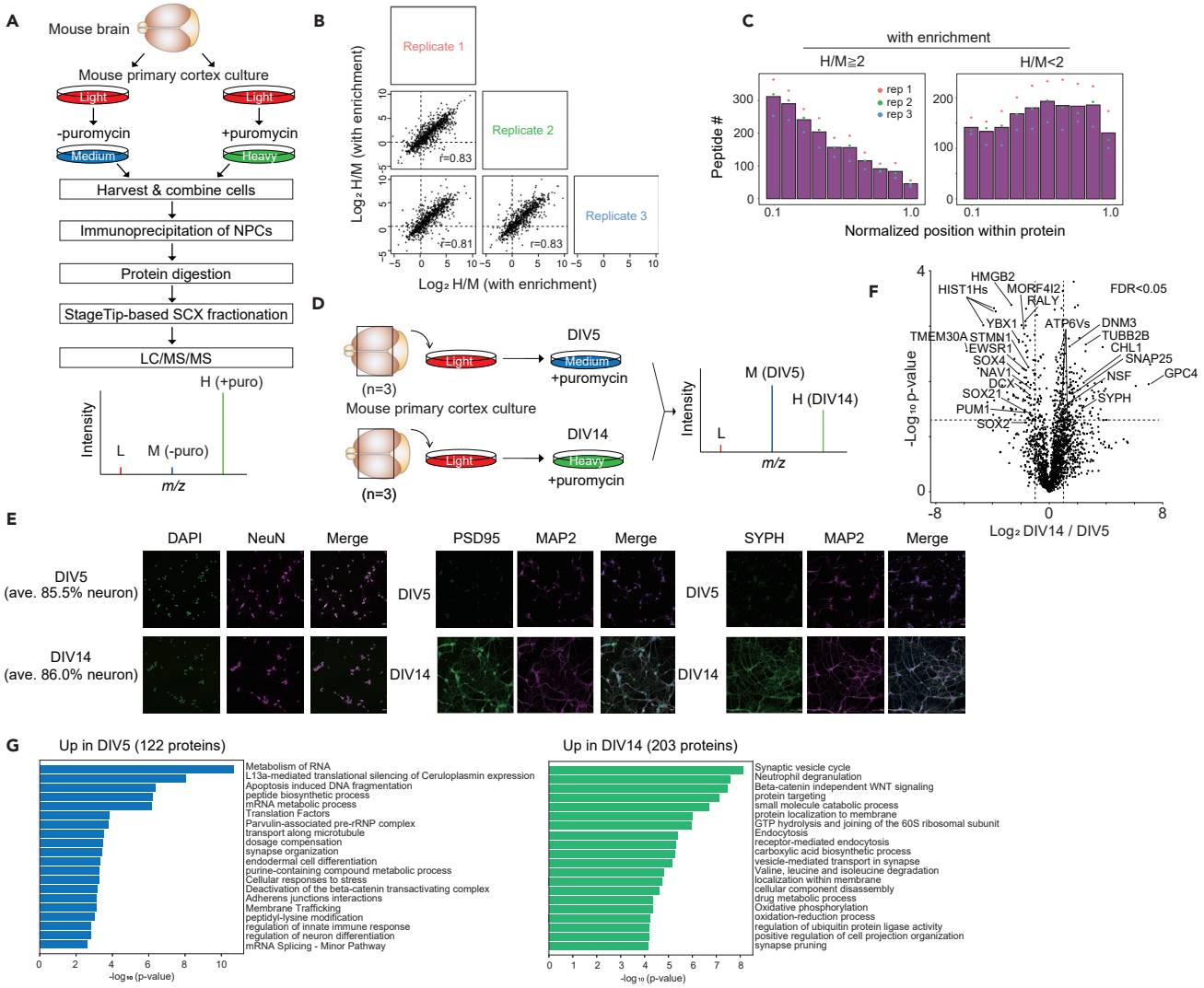

Figure 2. Application of pSNAP to mouse primary cortical neuronal cultures

(A) Schematic representation of the pSNAP workflow. Mouse primary cortical neurons are pulse labeled for 2 h with a combination of 10 μM puromycin and heavy amino acids or only medium-heavy amino acids. After IP of NPCs with anti-puromycin antibodies, NPCs are eluted with 0.15% TFA and digested into tryptic peptides. The resulting peptide sample is analyzed by LC/MS/MS.

(B) Multi-scatter plots of $\log_2$ H/M ratios from three independent experiments using mouse primary neurons.

(C) pSNAP can enrich NPCs from primary neurons. Relative starting positions of identified peptides within proteins. The bars represent averaged values from three independent experiments.

(D) Experimental design for the differential nascent proteome profiling of the mouse primary cultures between DIV 5 and 14.

(E) Representative images of primary neuronal cultures (DIV5 and DIV14) stained with DAPI (nuclear marker), NeuN (neuronal marker), MAP2 (dendritic microtubule marker), PSD95 (postsynaptic marker), and SYPH (presynaptic marker). Scale bar, 30 μm.

(F) A volcano plot showing differential NPC levels between DIV 5 and 14. Significantly regulated proteins were identified based on a combination of the *t*-test p-value ($p < 0.05$) of three replicates and the mean of the SILAC ratios [above 0.5 (a $\log_2$ ratio)] (dash lines) which correspond to FDR <0.05 (see STAR Methods).

(G) Gene ontology enrichment analyses for the significantly upregulated NPCs (adjusted $p < 0.01$).

applied pSNAP to characterize the global impact of a kinase inhibitor on cellular translation. We focused on casein kinase 2 (CK2) as it is ubiquitously expressed in all cells, and has been implicated in translational control through phosphorylation of specific eukaryotic initiation factors (eIFs) (Gandin et al., 2016; Lamper et al., 2020). However, the protein targets of translational regulation by CK2 remain unknown. Therefore, HeLa cells were pre-incubated with either DMSO or a specific CK2 inhibitor silmitasertib (also known as CX4945) (Siddiqui-Jain et al., 2010) for 10 min (Figure 3A), and then pulse-labeled with puromycin and

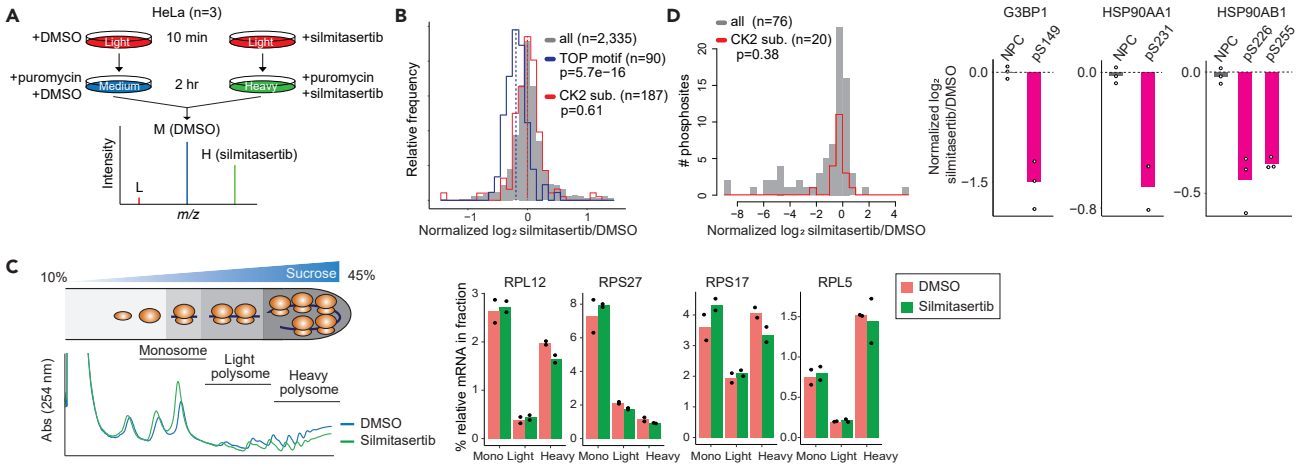

Figure 3. Quantitative analysis of translational responses and nascent phosphorylation

(A) Experimental design for global analysis of translational changes induced by a CK2 inhibitor silmitasertib (10 μM).

(B) A histogram of $\log_2$ fold changes [H/M (silmitasertib/DMSO) ratios] of protein synthesis induced by silmitasertib. Averaged $\log_2$ H/M ratios based on proteins quantified in at least two of the three replicates are shown. Results from individual replicates are shown in Figure 3B. A subset of proteins whose mRNAs contain a TOP motif is shown in dark blue. CK2 substrates determined by an *in vitro* kinase reaction (Sugiyama et al., 2019) are shown in red. All quantified proteins are shown in gray. The dashed lines indicate median values of the three groups (all, TOP motif, and CK2 substrates) The p-value was computed using the two-sided Wilcoxon rank-sum test.

(C) qRT-PCR validation of pSNAP result. (Left panel) Representative polysome profiles of HeLa cells treated with DMSO or silmitasertib. (Right panel) Polysomal association of mRNAs encoding for the selected ribosomal proteins that were repressed upon CK2 inhibition according to pSNAP.

(D) CK2 inhibition led to decreased phosphorylation levels of nascent forms of known CK2 substrates. (Left panel) A histogram of $\log_2$ fold changes [H/M (silmitasertib/DMSO) ratios] of phosphorylation sites induced by silmitasertib. Averaged $\log_2$ H/M ratios based on class I phosphosites quantified in at least one of the three replicates are shown. CK2 substrates determined by *in vitro* kinase reaction (Sugiyama et al., 2019) are shown in red. All quantified proteins are shown in gray. The p-value was computed using the two-sided Wilcoxon rank-sum test. (Right panel) Change of NPC and phosphorylation levels due to silmitasertib treatment versus DMSO treatment. The indicated phosphorylation sites of G3BP1, HSP90AA1, and HSP90AB1 are known CK2 substrates. Levels of the NPCs were quantified from NPC-derived unphosphorylated peptides. The bars represent averaged values from two or three replicates.

SILAC amino acids for 2 h in the presence of DMSO or silmitasertib, and processed as illustrated in Figure 1B. H/M ratios in MS spectra represent the difference in production of NPCs between the two conditions (silmitasertib and DMSO treatments). We first confirmed that NPCs could be enriched; H- and M-labeled peptides both exhibited the trend of protein N-terminus-biased positions (Figure S3A).

To understand the gene expression networks at the NPC level, we first asked whether *in vitro* CK2 substrates (Sugiyama et al., 2019) might be regulated translationally, but found no evidence to support this (Figure 3B and Table S4). On the one hand, a recent study showed that CK2 acts in concert with mTORC1 (Gandin et al., 2016) and regulates the translation of mRNAs containing 5′ terminal oligopyrimidine (TOP) motifs (Hsieh et al., 2012; Thoreen et al., 2012). We therefore asked whether the inhibition of CK2 affects the translation of TOP mRNAs. Indeed, we found that CK2 inhibition led to marked repression of NPCs with a TOP motif in their mRNAs (p = 5.7e-16), encoding for components of the translational machinery such as ribosomal proteins (Figures 3B and S3B for individual replicates).

To validate this, we performed quantitative real-time qRT-PCR analysis of mRNAs encoding for the selected silmitasertib-sensitive ribosomal proteins (average $\log_2$ fold-change, RPL12: −0.52, RPS27: −0.54, RPS17: −0.16, RPL5: −0.18) from monosome, light, and heavy polysome fractions (Figure 3C left panel). The polysome profiles revealed that silmitasertib induced a slight reduction in the polysomes (Figure 3C left panel), indicating that CK2 inhibition leads to translational repression. The silmitasertib-sensitive group (RPL12, RPS27, and RPS17 but not RPL5) tended to be less abundant in the heavy polysome fraction than in the monosome fraction (Figure 3C right panel), in agreement with the pSNAP result (Figure 3B). Although qRT-PCR confirmed the general trend in translational regulation revealed by pSNAP, there was no correlation between the effect sizes measured with pSNAP and those observed with qRT-PCR. This may be due to technical differences between methods (mass spectrometry or PCR) and analytes [elongating nascent polypeptides (pSNAP) or ribosome-associated mRNA (qRT-PCR)].

TOP mRNAs are well known targets that are subject to selective translation through mTORC1 (Hsieh et al., 2012; Thoreen et al., 2012). Hence, this result supports the idea that CK2 may regulate the translation of TOP mRNAs in concert with mTORC1, in line with a previous report that CK2 enhances mTORC1 activity (Gandin et al., 2016). In sum, our analysis uncovered acute translational responses to silmitasertib via the CK2 and mTOR pathways, which may contribute to further understanding of the mechanism of action of silmitasertib, a promising molecular therapy for several types of cancers (phase II) (Siddiqui-Jain et al., 2010) as well as SARS-CoV-2 infection (Bouhaddou et al., 2020).

Profiling modifications on nascent proteins

The present method not only enables the global profiling of NPCs but also highlights the modifications of NPCs that might be co-translationally regulated. Conventional proteomic approaches cannot resolve modifications on nascent and matured proteins, and so the distribution of the two types of modifications within a protein goes undetected; yet the timing of modifications can be important for protein processing (Aksnes et al., 2019; Varland et al., 2015) such as folding (Keshwani et al., 2012; Kii et al., 2016). In the silmitasertib treatment experiment (Figure 3), we identified 127 unique phosphopeptides without phosphopeptide enrichment. Among them, 76 class I phosphosites (localization probability >0.75) (Olsen et al., 2006) that were quantified in at least one of the three replicates are shown in Figure 3D. We found that CK2 inhibition led to decreased phosphorylation levels on nascent forms of known CK2 substrates, such as G3BP1 pS149 (Reineke et al., 2017), HSP90AA1 pS231, and HSP90AB1 pS226, pS255 (Mollapour and Neckers, 2012), while no marked change was observed at the NPC level (Figure 3D right panel and Table S4). On the one hand, we found that phosphorylation of most of the CK2 substrates was not reduced by the inhibitor (Figure 3D left panel), indicating that phosphorylation of NPCs may be differentially regulated from that of mature proteins. Hence, CK2 may act in close proximity to the ribosome to co-translationally phosphorylate specific nascent proteins, possibly regulating protein stability through phosphorylation of newly made proteins, as observed for XRCC1 (Parsons et al., 2010) and CFTR (Pankow et al., 2019).

Protein N-terminal (Nt) acetylation is one well-studied "co-translational" modification (Aksnes et al., 2019; Yeom et al., 2017); however, recent studies have revealed "post-translational" Nt-acetylation on many transmembrane proteins and actin (Yeom et al., 2017). While earlier N-terminomics studies identified thousands of protein Nt-acetylation sites (Choudhary et al., 2014; Lai et al., 2015; Yeom et al., 2017), it remains unclear whether these sites are co- or post-translationally modified. We thus sought to apply pSNAP to pinpoint Nt-acetylation sites on NPCs with high accuracy. For this purpose, HeLa cells were treated with either 100 μg/mL cycloheximide (CHX) or DMSO for 2 h in the presence of 10 μM puromycin and corresponding SILAC amino acid pairs. By combining pSNAP with low pH strong cation exchange (SCX) chromatography (Helbig et al., 2010), we enriched Nt-acetylated peptides that were eluted in the flow-through fraction and early in SCX fractionation due to the loss of positive charge at their N-terminal ends (Figure 4A). We confirmed that the NPCs could be enriched (Figure S4 and Table S5) and identified 298 unique protein Nt-acetylated sites that exhibited H/M (DMSO/CHX) $\geqq 2$ in at least one of the three replicates (Table S5). Notably, beta-actin's Nt-acetylation showed H/M < 1 in all replicates, indicating that it occurs post-translationally, in agreement with a previous report (Drazic et al., 2018). To better understand acceptor sites for Nt-acetylation on NPCs, we focused on amino acids at the second residue [next to the initiator methionine (iMet)] (Figure 4B). In accordance with the substrate specificity of major N-terminal acetyltransferases (Aksnes et al., 2019; Yeom et al., 2017) and known Nt-acetylation sites from the Uniprot human database, we observed a high prevalence of alanine, serine, and threonine for Nt-acetylated NPCs whose iMet was cleaved, while the acidic amino acids (aspartic acid and glutamic acid) and phenylalanine were overrepresented in the iMet-retained and Nt-acetylated NPCs (Figure 4B). We did not observe a significant difference in acceptor amino acids between NPCs and the input.

Protein N-terminal modifications on a nascent protein can modulate binding partners

Protein N-termini are hotspots for modifications during translation and thus can regulate co-translational events such as folding and degradation through interactions with proteins (Collart and Weiss, 2020). We next sought to discover cross-talk between protein Nt-acetylation and other modifications on NPCs as the combination of different types of modifications confers additional specificity and combinatorial logic to protein interactions. We searched our dataset focusing on phosphorylation, which can function as a versatile switch to modulate protein interactions. We identified 134 phosphorylated peptides in the Nt-acetylation-enriched samples. Among them, we focused on phosphorylation at Ser19 of histone H1.5 (H1.5) co-occurring with protein Nt-acetylation within the same peptide (Figure 4C). Peptide-level

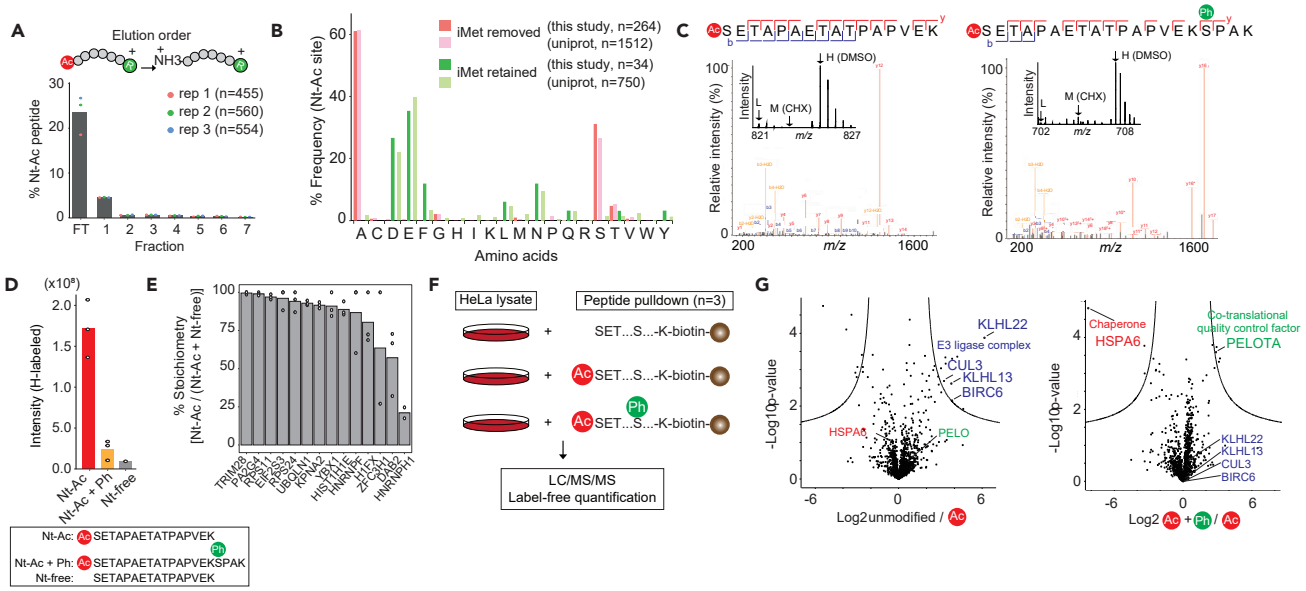

Figure 4. Characterization of protein Nt-acetylation and phosphorylation on nascent proteins

(A) Enrichment of Nt-acetylated peptides with SCX-based fractionation. The percentage of the number of protein Nt-acetylated peptides in all peptides identified in individual fractions is shown. The bars represent averaged values from three replicates.

(B) The amino acid frequency at the second residue next to iMet of acetylated protein N-termini based on the absence (pink) or presence (green) of iMet. Only nascent proteins that showed H/M> 2 in at least one of the three replicates were considered. For comparison, the human proteome from the SwissProt protein database is shown (light pink and light green indicate iMet-removed and iMet-retained sites, respectively).

(C) Representative MS/MS spectra of Ac-SETAPAETATPAPVEK (left) and Ac-SETAPAETATPAPVEKpSPAK (right) from histone H1.5. The insets show representative MS spectra of corresponding peptides and demonstrate that the protein Nt-acetylation and adjacent phosphorylation occurred on nascent H1.5.

(D) Quantification of H-labeled peptide intensities from Nt-acetylated (red), Nt-acetylated and phosphorylated (orange), and Nt-unmodified (gray) forms.

(E) Stoichiometry (%) of protein Nt-acetylation estimated based on intensities of H-labeled peptides from Nt-acetylated and counterpart (unmodified) forms. The bars represent averaged values from two or three replicates.

(F) Experimental design for peptide-pulldown assays using three different peptide probes. Nt-unmodified, Nt-acetylated, or Nt-acetylated and phosphorylated biotinylated peptides corresponding to amino acid residues from 2 to 22 (SETAPAETATPAPVEKSPAKK) of H1.5 were conjugated to streptavidin agarose resins. Beads were incubated with HeLa cell lysate, and eluted for LC/MS/MS analysis.

(G) Volcano plots from the pulldown assays of Nt-free vs Nt-acetylated peptides (left) and Nt-acetylated vs Nt-acetylated and phosphorylated peptides (right) are shown. The cutoff curve indicates false discovery rate (FDR) < 0.05, S0>2.

quantification of H-labeled peptides indicated that the Nt-acetylated form (Ac-SETAPAETATPAPVEK) is a major nascent proteoform of H1.5 in comparison to the Nt-acetylated and phosphorylated form (Ac-SETAPAETATPAPVEKpSPAK) and the unmodified form (SETAPAETATPAPVEK) (Figure 4D). Because the trypsin cleavage site (Lys18) is next to the phosphorylation site (Ser19), the phosphorylated form was exclusively observed as a missed cleavage peptide due to the inaccessibility of trypsin. We therefore used the no-missed-cleavage peptide (SETAPAETATPAPVEK) as an unmodified counterpart for the "missed-cleavage phosphopeptide" (Ac-SETAPAETATPAPVEKpSPAK) in the quantification shown in Figure 4D. Such highly stoichiometric patterns of nascent Nt-acetylation were also seen for the 13 sites whose Nt-acetylated and counterpart (unmodified) peptides were both quantified (Figure 4E), in marked contrast to the very low (median 0.02%) stoichiometry of lysine acetylation in HeLa cells (Hansen et al., 2019).

To understand the role of the nascent modifications and their impacts on protein interactions, we performed peptide-based pulldown experiments on HeLa cell lysate using three distinct peptide probes that mimic 1) Nt-unmodified, 2) Nt-acetylated, or 3) Nt-acetylated and phosphorylated forms of H1.5 (Figure 4F). The peptide-based screen revealed proteins that differentially interacted with the specific peptide probes (Figure 4G and Table S6). One prominent example is a ubiquitin E3 ligase complex (KLHL13, KLHL22, CUL3, and BIRC6) that showed a robust interaction with the unmodified peptides (Figure 4G left panel). Thus, Nt-unmodified H1.5 is likely to be degraded through the ubiquitin-proteasome system, which may explain why the Nt-unmodified H1.5 was markedly less abundant than the acetylated forms in HeLa cells (Figure 4D). Accordingly, protein Nt-acetylation of H1.3 is protective against protein

degradation, in line with the idea that Nt-acetylated mitochondrial proteins bearing inhibitor of apoptosis-binding (IAP) motifs are shielded from the IAP family of E3 ubiquitin ligases (Mueller et al., 2021). Interestingly, the Nt-acetylated and phosphorylated version of the peptide preferentially bound a co-translational quality control factor PELOTA while disfavoring the interaction with a molecular chaperone HSPA6 (Figure 4G right panel). PELOTA was shown to promote the dissociation of stalled ribosomes and the release of intact peptidyl-tRNA for ribosome recycling (Pisareva et al., 2011). Thus, the nascent H1.5 phosphorylation in the N-terminal region may represent an additional "modification code" to recruit PELOTA and to repel HSPA6 as a surveillance mechanism for aberrant nascent H1.5. In summary, pSNAP enables us to uncover modifications on NPCs that may represent a new layer of translational control, i.e., one shaped by nascent protein modifications.

Conclusions

The pSNAP approach presented here offers multiple advantages over currently available methods for capturing nascent polypeptide chains and their modifications, which represent a hidden layer in understanding translational regulations in cell biology that is inaccessible by conventional ribosome profiling or proteomic approaches. The advantage of pSNAP lies in the use of dual-pulse labeling. The incorporation of puromycin facilitates the enrichment of NPCs from a complex background, and the use of pulsed SILAC enables both protein quantification and discrimination of nascent from pre-existing proteins. Moreover, the experimental workflow is simple in contrast to existing methods that involve ribosome purification using ultracentrifugation (Aviner et al., 2013) and/or chemical labeling steps (Forester et al., 2018; Huang et al., 2021; Tong et al., 2020; Uchiyama et al., 2020). In addition, the method does not require special puromycin derivatives such as biotin-puromycin (Aviner et al., 2013) or clickable puromycin (Forester et al., 2018; Huang et al., 2021; Tong et al., 2020; Uchiyama et al., 2020). Our results show that pSNAP can quantify changes in NPC levels in response to environmental cues, and is useful for characterizing nascent modifications. In addition, this method could be applied to identify the NPC interactome during translation since some proteins appear to form homo- (Bertolini et al., 2021) or hetero (Kamenova et al., 2019) complexes in a co-translational manner.

Limitations of the study

While puromycin or its analog has been used to analyze protein synthesis in many cell lines and model systems (Aviner, 2020), it may also cause a secondary effect on cellular translation (Marciano et al., 2018). In this study, we therefore used a relatively low concentration of puromycin that did not affect cell viability or degradation of puromycylated proteins, at least in HeLa cells, but further investigations would be required to characterize the mode of action of puromycin in detail. We demonstrated that pSNAP is readily applicable to a cell line and to primary-cultured cells, though further development will be needed for its application to *in vivo* systems. For example, the direct enrichment and proteomic analysis of puromycylated peptides digested from NPCs provides a signature of genuine NPCs, and would not require pulse SILAC labeling.

While we successfully characterized protein Nt-acetylation and phosphorylation at the NPC level, we cannot rule out the possibility of modifications to the released puromycylated NPCs from ribosomes. Further structural analysis and co-localization studies may provide further clarification. Also, since the amount of NPCs obtained by pSNAP is limited (considered to be <1 μg based on the total ion chromatogram), the method cannot readily be combined with a biochemical enrichment technique for modified peptides. Further improvement of the current pSNAP protocol to increase sensitivity is desirable for capturing omics-level modification sites. As shown in Figure 3C, perturbation of cells may cause global changes in translation. However, such global changes would not be detected in a typical proteome analysis because ratios are normalized based on the assumption that abundance of most proteins remains unchanged under two conditions. We also detected M-channel-derived signals for some proteins even without puromycin (Figures 1D and 2B). Hence, background noise due to non-specific proteins may compress quantitative ratios in experiments comparing two conditions based on H/M ratios (see e.g., Figures 2D and 3A), leading to systematic underestimation of quantitative ratios.

STAR★METHODS

Detailed methods are provided in the online version of this paper and include the following:

- KEY RESOURCES TABLE
- RESOURCE AVAILABILITY
  - Lead contact

SUPPLEMENTAL INFORMATION

Supplemental information can be found online at https://doi.org/10.1016/j.isci.2022.104516.

ACKNOWLEDGMENTS

We are very grateful to Erik McShane (Harvard Medical School), Matthew L Kraushar (Max Planck Institute for Molecular Genetics), and Tatsuya Niwa (Tokyo Institute of Technology) for critical reading of the manuscript. We thank Takuya Uehata and Osamu Takeuchi for providing cultured cells. We thank the members of the Department of Molecular & Cellular BioAnalysis, the Department of Proteomics, Drug Discovery, Makoto Arita, Shinya Oki, Yosuke Isobe, Masashi Maekawa, Yasuhiro Murakawa, and Hiroshi Tsugawa for fruitful discussion. KI thanks the Samuro Kakiuchi Memorial Research Award for Young Scientists for supporting this study. This work was supported by JSPS Grant-in-Aid for Scientific Research (Grant Numbers 18K14674, 20H03241, 20H04844, 21H05720 to KI and 17H05667 to YI), JST PRESTO (JPMJPR18H2), JST FOREST (JPMJFR214L), JST ERATO (JPMJER2101), the Takeda Science Foundation to KI and DOW, AMED (18dm0307023h) to DOW, JST Strategic Basic Research Program CREST (18070870), and AMED Advanced Research and Development Programs for Medical Innovation CREST (18068699) to YI.

AUTHOR CONTRIBUTIONS

Conceptualization & Methodology, J.U., Y.I., and K.I.; Investigation, J.U., R.R., K.M., Y.K., M.I., Y.M., D.O.W., Y.C., Y. I., and K.I; Resources, D.O.W., M.I, Y.M., Y.I., and K.I.; Writing - Original Draft, K.I.; Writing - Review & Editing, J.U., R.R., K.M., M.I. Y.M., D.O.W., Y.I.; Supervision, Y.I. and K.I.

DECLARATION OF INTERESTS

The authors declare no competing interests.

Received: July 4, 2021
Revised: February 10, 2022
Accepted: May 31, 2022
Published: July 15, 2022

REFERENCES

Adachi, J., Hashiguchi, K., Nagano, M., Sato, M., Sato, A., Fukamizu, K., Ishihama, Y., and Tomonaga, T. (2016). Improved proteome and phosphoproteome analysis on a cation exchanger by a combined acid and salt gradient. Anal. Chem. *88*, 7899–7903. https://doi.org/10.1021/acs.analchem.6b01232.

Aksnes, H., Ree, R., and Arnesen, T. (2019). Co-translational, post-translational, and non-catalytic roles of N-terminal acetyltransferases. Mol. Cell *73*, 1097–1114. https://doi.org/10.1016/j.molcel.2019.02.007.

Aviner, R. (2020). The science of puromycin: from studies of ribosome function to applications in biotechnology. Comput. Struct. Biotechnol. J. *18*, 1074–1083. https://doi.org/10.1016/j.csbj.2020.04.014.

Aviner, R., Geiger, T., and Elroy-Stein, O. (2013). Novel proteomic approach (PUNCH-P) reveals cell cycle-specific fluctuations in mRNA translation. Genes Dev. *27*, 1834–1844. https://doi.org/10.1101/gad.219105.113.

Aviner, R., Li, K.H., Frydman, J., and Andino, R. (2021). Cotranslational prolyl hydroxylation is essential for flavivirus biogenesis. Nature *596*, 558–564. https://doi.org/10.1038/s41586-021-03851-2.

Bertolini, M., Fenzl, K., Kats, I., Wruck, F., Tippmann, F., Schmitt, J., Auburger, J.J., Tans, S., Bukau, B., and Kramer, G. (2021). Interactions between nascent proteins translated by adjacent ribosomes drive homomer assembly. Science *371*, 57–64. https://doi.org/10.1126/science.abc7151.

Bogdanow, B., Schmidt, M., Weisbach, H., Gruska, I., Vetter, B., Imami, K., Ostermann, E., Brune, W., Selbach, M., Hagemeier, C., and Wiebusch, L. (2020). Cross-regulation of viral kinases with cyclin A secures shutoff of host DNA synthesis. Nat. Commun. *11*, 4845. https://doi.org/10.1038/s41467-020-18542-1.

Bouhaddou, M., Memon, D., Meyer, B., White, K.M., Rezelj, V.V., Correa Marrero, M., Polacco, B.J., Melnyk, J.E., Ulferts, S., Kaake, R.M., et al. (2020). The global phosphorylation landscape of SARS-CoV-2 infection. Cell *182*, 685–712.e19. https://doi.org/10.1016/j.cell.2020.06.034.

Choudhary, C., Weinert, B.T., Nishida, Y., Verdin, E., and Mann, M. (2014). The growing landscape of lysine acetylation links metabolism and cell signalling. Nat. Rev. Mol. Cell Biol. *15*, 536–550. https://doi.org/10.1038/nrm3841.

Collart, M.A., and Weiss, B. (2020). Ribosome pausing, a dangerous necessity for co-translational events. Nucleic Acids Res. *48*, 1043–1055. https://doi.org/10.1093/nar/gkz763.

Cox, J., and Mann, M. (2008). MaxQuant enables high peptide identification rates, individualized p.p.b.-range mass accuracies and proteome-wide protein quantification. Nat. Biotechnol. *26*, 1367–1372. https://doi.org/10.1038/nbt.1511.

Cox, J., Neuhauser, N., Michalski, A., Scheltema, R.A., Olsen, J.V., and Mann, M. (2011). Andromeda: a peptide search engine integrated into the MaxQuant environment. J. Proteome Res. *10*, 1794–1805. https://doi.org/10.1021/pr101065j.

Dieterich, D.C., Link, A.J., Graumann, J., Tirrell, D.A., and Schuman, E.M. (2006). Selective identification of newly synthesized proteins in mammalian cells using bioorthogonal noncanonical amino acid tagging (BONCAT). Proc. Natl. Acad. Sci. U S A. *103*, 9482–9487. https://doi.org/10.1073/pnas.0601637103.

Doherty, M.K., Hammond, D.E., Clague, M.J., Gaskell, S.J., and Beynon, R.J. (2009). Turnover of the human proteome: determination of protein intracellular stability by dynamic SILAC. J. Proteome Res. *8*, 104–112. https://doi.org/10.1021/pr800641v.

Drazic, A., Aksnes, H., Marie, M., Boczkowska, M., Varland, S., Timmerman, E., Foyn, H., Glomnes, N., Rebowski, G., Impens, F., et al. (2018). NAA80 is actin's N-terminal acetyltransferase and regulates cytoskeleton assembly and cell motility. Proc. Natl. Acad. Sci. U S A. *115*, 4399–4404. https://doi.org/10.1073/pnas.1718336115.

Eichelbaum, K., Winter, M., Diaz, M.B., Herzig, S., and Krijgsveld, J. (2012). Selective enrichment of newly synthesized proteins for quantitative secretome analysis. Nat. Biotechnol. *30*, 984–990. https://doi.org/10.1038/nbt.2356.

Forester, C.M., Zhao, Q., Phillips, N.J., Urisman, A., Chalkley, R.J., Oses-Prieto, J.A., Zhang, L., Ruggero, D., and Burlingame, A.L. (2018). Revealing nascent proteomics in signaling pathways and cell differentiation. Proc. Natl. Acad. Sci. U S A. *115*, 2353–2358. https://doi.org/10.1073/pnas.1707514115.

Frese, C.K., Mikhaylova, M., Stucchi, R., Gautier, V., Liu, Q., Mohammed, S., Heck, A.J.R., Altelaar, A.M., Altelaar, A.F.M., and Hoogenraad, C.C. (2017). Quantitative map of proteome dynamics during neuronal differentiation. Cell Rep. *18*, 1527–1542. https://doi.org/10.1016/j.celrep.2017.01.025.

Gandin, V., Masvidal, L., Cargnello, M., Gyenis, L., McLaughlan, S., Cai, Y., Tenkerian, C., Morita, M., Balanathan, P., Jean-Jean, O., et al. (2016). mTORC1 and CK2 coordinate ternary and eIF4F complex assembly. Nat. Commun. *7*, 11127. https://doi.org/10.1038/ncomms11127.

Hansen, B.K., Gupta, R., Baldus, L., Lyon, D., Narita, T., Lammers, M., Choudhary, C., and Weinert, B.T. (2019). Analysis of human acetylation stoichiometry defines mechanistic constraints on protein regulation. Nat. Commun. *10*, 1055. https://doi.org/10.1038/s41467-019-09024-0.

Hebert, A.S., Prasad, S., Belford, M.W., Bailey, D.J., McAlister, G.C., Abbatiello, S.E., Huguet, R., Wouters, E.R., Dunyach, J.-J., Brademan, D.R., et al. (2018). Comprehensive single-shot proteomics with FAIMS on a hybrid Orbitrap mass spectrometer. Anal. Chem. *90*, 9529–9537. https://doi.org/10.1021/acs.analchem.8b02233.

Helbig, A.O., Gauci, S., Raijmakers, R., van Breukelen, B., Slijper, M., Mohammed, S., and Heck, A.J.R. (2010). Profiling of N-acetylated protein termini provides in-depth insights into the N-terminal nature of the proteome. Mol. Cell. Proteomics *9*, 928–939. https://doi.org/10.1074/mcp.m900463-mcp200.

Howden, A.J.M., Geoghegan, V., Katsch, K., Efstathiou, G., Bhushan, B., Boutureira, O., Thomas, B., Trudgian, D.C., Kessler, B.M., Dieterich, D.C., et al. (2013). QuaNCAT: quantitating proteome dynamics in primary cells. Nat. Methods *10*, 343–346. https://doi.org/10.1038/nmeth.2401.

Hsieh, A.C., Liu, Y., Edlind, M.P., Ingolia, N.T., Janes, M.R., Sher, A., Shi, E.Y., Stumpf, C.R., Christensen, C., Bonham, M.J., et al. (2012). The translational landscape of mTOR signalling steers cancer initiation and metastasis. Nature *485*, 55–61. https://doi.org/10.1038/nature10912.

Huang, Y., Zhang, Q., Yang, L., Lin, L., Xie, J., Yao, J., Zhou, X., Zhang, L., Shen, H., and Yang, P. (2021). Puromycin-modified silica microsphere-based nascent proteomics method for rapid and deep nascent proteome profile. Anal. Chem. *93*, 6403–6413. https://doi.org/10.1021/acs.analchem.0c05393.

Imami, K., Milek, M., Bogdanow, B., Yasuda, T., Kastelic, N., Zauber, H., Ishihama, Y., Landthaler, M., and Selbach, M. (2018). Phosphorylation of the ribosomal protein RPL12/uL11 affects translation during mitosis. Mol. Cell *72*, 84–98.e9. https://doi.org/10.1016/j.molcel.2018.08.019.

Imami, K., Sugiyama, N., Tomita, M., and Ishihama, Y. (2010). Quantitative proteome and phosphoproteome analyses of cultured cells based on SILAC labeling without requirement of serum dialysis. Mol. Biosyst. *6*, 594–602. https://doi.org/10.1039/b921379a.

Ingolia, N.T., Ghaemmaghami, S., Newman, J.R.S., and Weissman, J.S. (2009). Genome-wide analysis in vivo of translation with nucleotide resolution using ribosome profiling. Science *324*, 218–223. https://doi.org/10.1126/science.1168978.

Ishihama, Y., Rappsilber, J., Andersen, J.S., and Mann, M. (2002). Microcolumns with self-assembled particle frits for proteomics. J. Chromatogr. A *979*, 233–239. https://doi.org/10.1016/s0021-9673(02)01402-4.

Kaech, S., and Banker, G. (2006). Culturing hippocampal neurons. Nat. Protoc. *1*, 2406–2415. https://doi.org/10.1038/nprot.2006.356.

Kamenova, I., Mukherjee, P., Conic, S., Mueller, F., El-Saafin, F., Bardot, P., Garnier, J.-M., Dembele, D., Capponi, S., Timmers, H.T.M., et al. (2019). Co-translational assembly of mammalian nuclear multisubunit complexes. Nat. Commun. *10*, 1740. https://doi.org/10.1038/s41467-019-09749-y.

Keshwani, M.M., Klammt, C., von Daake, S., Ma, Y., Kornev, A.P., Choe, S., Insel, P.A., and Taylor, S.S. (2012). Cotranslational cis-phosphorylation of the COOH-terminal tail is a key priming step in the maturation of cAMP-dependent protein kinase. Proc. Natl. Acad. Sci. U S A. *109*, E1221–E1229. https://doi.org/10.1073/pnas.1202741109.

Kii, I., Sumida, Y., Goto, T., Sonamoto, R., Okuno, Y., Yoshida, S., Kato-Sumida, T., Koike, Y., Abe, M., Nonaka, Y., et al. (2016). Selective inhibition of the kinase DYRK1A by targeting its folding process. Nat. Commun. *7*, 11391. https://doi.org/10.1038/ncomms11391.

Klann, K., Tascher, G., and Münch, C. (2020). Functional translatome proteomics reveal Converging and dose-dependent regulation by mTORC1 and eIF2α. Mol. Cell *77*, 913–925.e4. https://doi.org/10.1016/j.molcel.2019.11.010.

Lai, Z.W., Petrera, A., and Schilling, O. (2015). Protein amino-terminal modifications and proteomic approaches for N-terminal profiling. Curr. Opin. Chem. Biol. *24*, 71–79. https://doi.org/10.1016/j.cbpa.2014.10.026.

Lamper, A.M., Fleming, R.H., Ladd, K.M., and Lee, A.S.Y. (2020). A phosphorylation-regulated eIF3d translation switch mediates cellular adaptation to metabolic stress. Science *370*, 853–856. https://doi.org/10.1126/science.abb0993.

Marciano, R., Leprivier, G., and Rotblat, B. (2018). Puromycin labeling does not allow protein synthesis to be measured in energy-starved cells. Cell Death Dis. *9*, 1–3. https://doi.org/10.1038/s41419-017-0056-x.

Masuda, T., Tomita, M., and Ishihama, Y. (2008). Phase transfer surfactant-aided trypsin digestion for membrane proteome analysis. J. Proteome Res. *7*, 731–740. https://doi.org/10.1021/pr700658q.

McShane, E., Sin, C., Zauber, H., Wells, J.N., Donnelly, N., Wang, X., Hou, J., Chen, W., Storchova, Z., Marsh, J.A., et al. (2016). Kinetic analysis of protein stability reveals age-dependent degradation. Cell *167*, 803–815.e21. https://doi.org/10.1016/j.cell.2016.09.015.

Mellacheruvu, D., Wright, Z., Couzens, A.L., Lambert, J.-P., St-Denis, N.A., Li, T., Miteva, Y.V., Hauri, S., Sardiu, M.E., Low, T.Y., et al. (2013). The CRAPome: a contaminant repository for affinity purification-mass spectrometry data. Nat. Methods *10*, 730–736. https://doi.org/10.1038/nmeth.2557.

Miyamoto-Sato, E., Nemoto, N., Kobayashi, K., and Yanagawa, H. (2000). Specific bonding of puromycin to full-length protein at the C-terminus. Nucleic Acids Res. *28*, 1176–1182. https://doi.org/10.1093/nar/28.5.1176.

Mollapour, M., and Neckers, L. (2012). Post-translational modifications of Hsp90 and their contributions to chaperone regulation. Biochim. Biophys. Acta *1823*, 648–655. https://doi.org/10.1016/j.bbamcr.2011.07.018.

Moriya, Y., Kawano, S., Okuda, S., Watanabe, Y., Matsumoto, M., Takami, T., Kobayashi, D., Yamanouchi, Y., Araki, N., Yoshizawa, A.C., et al. (2019). The jPOST environment: an integrated proteomics data repository and database. Nucleic Acids Res. *47*, D1218–D1224. https://doi.org/10.1093/nar/gky899.

Mueller, F., Friese, A., Pathe, C., da Silva, R.C., Rodriguez, K.B., Musacchio, A., and Bange, T. (2021). Overlap of NatA and IAP substrates implicates N-terminal acetylation in protein stabilization. Sci. Adv. *7*, eabc8590. https://doi.org/10.1126/sciadv.abc8590.

Okuda, S., Watanabe, Y., Moriya, Y., Kawano, S., Yamamoto, T., Matsumoto, M., Takami, T., Kobayashi, D., Araki, N., Yoshizawa, A.C., et al. (2017). jPOSTrepo: an international standard data repository for proteomes. Nucleic Acids Res. *45*, D1107–D1111. https://doi.org/10.1093/nar/gkw1080.

Olsen, J.V., Blagoev, B., Gnad, F., Macek, B., Kumar, C., Mortensen, P., and Mann, M. (2006). Global, in vivo, and site-specific phosphorylation dynamics in signaling networks. Cell *127*, 635–648. https://doi.org/10.1016/j.cell.2006.09.026.

Pankow, S., Bamberger, C., and Yates, J.R., 3rd (2019). A posttranslational modification code for CFTR maturation is altered in cystic fibrosis. Sci. Signal. *12*, eaan7984. https://doi.org/10.1126/scisignal.aan7984.

Parsons, J.L., Dianova, I.I., Finch, D., Tait, P.S., Ström, C.E., Helleday, T., and Dianov, G.L. (2010). XRCC1 phosphorylation by CK2 is required for its stability and efficient DNA repair. DNA Repair *9*, 835–841. https://doi.org/10.1016/j.dnarep.2010.04.008.

Pisareva, V.P., Skabkin, M.A., Hellen, C.U.T., Pestova, T.V., and Pisarev, A.V. (2011). Dissociation by Pelota, Hbs1 and ABCE1 of mammalian vacant 80S ribosomes and stalled elongation complexes. EMBO J. *30*, 1804–1817. https://doi.org/10.1038/emboj.2011.93.

Reineke, L.C., Tsai, W.-C., Jain, A., Kaelber, J.T., Jung, S.Y., and Lloyd, R.E. (2017). Casein kinase 2 is linked to stress granule dynamics through phosphorylation of the stress granule nucleating protein G3BP1. Mol. Cell Biol. *37*, e00596-16. https://doi.org/10.1128/MCB.00596-16.

Schwanhäusser, B., Busse, D., Li, N., Dittmar, G., Schuchhardt, J., Wolf, J., Chen, W., and Selbach, M. (2011). Global quantification of mammalian gene expression control. Nature *473*, 337–342. https://doi.org/10.1038/nature10098.

Schwanhäusser, B., Gossen, M., Dittmar, G., and Selbach, M. (2009). Global analysis of cellular protein translation by pulsed SILAC. Proteomics *9*, 205–209. https://doi.org/10.1002/pmic.200800275.

Schwarz, A., and Beck, M. (2019). The benefits of cotranslational assembly: a structural perspective. Trends Cell Biol. *29*, 791–803. https://doi.org/10.1016/j.tcb.2019.07.006.

Siddiqui-Jain, A., Drygin, D., Streiner, N., Chua, P., Pierre, F., O'Brien, S.E., Bliesath, J., Omori, M., Huser, N., Ho, C., et al. (2010). CX-4945, an orally bioavailable selective inhibitor of protein kinase CK2, inhibits prosurvival and angiogenic signaling and exhibits antitumor efficacy. Cancer Res. *70*, 10288–10298. https://doi.org/10.1158/0008-5472.can-10-1893.

Stumpf, C.R., Moreno, M.V., Olshen, A.B., Taylor, B.S., and Ruggero, D. (2013). The translational landscape of the mammalian cell cycle. Mol. Cell *52*, 574–582. https://doi.org/10.1016/j.molcel.2013.09.018.

Sugiyama, N., Imamura, H., and Ishihama, Y. (2019). Large-scale discovery of substrates of the human kinome. Sci. Rep. *9*, 10503. https://doi.org/10.1038/s41598-019-46385-4.

Thoreen, C.C., Chantranupong, L., Keys, H.R., Wang, T., Gray, N.S., and Sabatini, D.M. (2012). A unifying model for mTORC1-mediated regulation of mRNA translation. Nature *485*, 109–113. https://doi.org/10.1038/nature11083.

Tong, M., Suttapitugsakul, S., and Wu, R. (2020). Effective method for accurate and sensitive quantitation of rapid changes of newly synthesized proteins. Anal. Chem. *92*, 10048–10057. https://doi.org/10.1021/acs.analchem.0c01823.

Tyanova, S., Temu, T., Sinitcyn, P., Carlson, A., Hein, M.Y., Geiger, T., Mann, M., and Cox, J. (2016). The Perseus computational platform for comprehensive analysis of (prote)omics data. Nat. Methods *13*, 731–740. https://doi.org/10.1038/nmeth.3901.

Uchiyama, J., Ishihama, Y., and Imami, K. (2020). Quantitative nascent proteome profiling by dual-pulse labelling with *O*-propargyl-puromycin and stable isotope-labelled amino acids. J. Biochem. *169*, 227–236. https://doi.org/10.1093/jb/mvaa104.

Varland, S., Osberg, C., and Arnesen, T. (2015). N-terminal modifications of cellular proteins: the enzymes involved, their substrate specificities and biological effects. Proteomics *15*, 2385–2401. https://doi.org/10.1002/pmic.201400619.

Yeom, J., Ju, S., Choi, Y., Paek, E., and Lee, C. (2017). Comprehensive analysis of human protein N-termini enables assessment of various protein forms. Sci. Rep. *7*, 6599. https://doi.org/10.1038/s41598-017-06314-9.

Zhou, Y., Zhou, B., Pache, L., Chang, M., Khodabakhshi, A.H., Tanaseichuk, O., Benner, C., and Chanda, S.K. (2019). Metascape provides a biologist-oriented resource for the analysis of systems-level datasets. Nat. Commun. *10*, 1523. https://doi.org/10.1038/s41467-019-09234-6.

STAR★METHODS

KEY RESOURCES TABLE

REAGENT or RESOURCE	SOURCE	IDENTIFIER
Antibodies		
mouse anti-puromycin antibody (clone 12D10) (IP)	Merck	Cat# MABE343, RRID:AB_2566826
mouse anti-puromycin antibody (clone 3RH11) (1:5,000)	Cosmo Bio	Cat# CAC-PEN-MA001, RRID:AB_2620162
rabbit anti-ubiquitin antibody (1:2,000)	Cell Signaling Technology	Cat# 3933, RRID:AB_2180538
Chemicals, peptides, and recombinant proteins		
puromycin dihydrochloride	FUJIFILM Wako	Cat# 160-23,151
L-($^{13}C_6$,$^{15}N_4$)-arginine (Arg"10")	Cambridge Isotope Laboratories	Cat# CNLM-539-H
L-($^{13}C_6$,$^{15}N_2$)-lysine (Lys"8")	Cambridge Isotope Laboratories	Cat# CNLM-291-H
L-($^{15}N_4$)-arginine (Arg"4")	Cambridge Isotope Laboratories	Cat# LM-396
L-(D_4)-lysine (Lys"4")	Cambridge Isotope Laboratories	Cat# DLM-2640
MG-132	Chemscene	Cat# CS-0471
Bortezomib	FUJIFILM Wako	Cat# 021-18901
Silmitasertib	MedChemExpress	Cat# HY-50855
cycloheximide (CHX)	FUJIFILM Wako	Cat# 037-20991
fetal bovine serum (FBS)	Thermo Fisher Scientific	Cat#10270106
DMEM(High Glucose) with L-Glutamine, Phenol Red and Sodium Pyruvate	FUJIFILM Wako	Cat# 043-30085
arginine- and lysine-free Neurobasal-A medium	Research Institute for the Functional Peptides	N/A
DMEM for SILAC	Thermo Fisher Scientific	Cat# 88364
neuron dissociation solutions	FUJIFILM Wako	Cat#291-78001
poly-L-lysine	Merck	Cat#A-005-C
MEM	Thermo Fisher Scientific	Cat#11095080
D-glucose	Merck	Cat#108337
sodium pyruvate	Nacalai Tesque	Cat#06977-34
penicillin-streptomycin	Thermo Fisher Scientific	Cat#15140122
Neurobasal-A medium	Thermo Fisher Scientific	Cat#10888022
B-27 supplement	Thermo Fisher Scientific	Cat#17504044
GlutaMAX	Thermo Fisher Scientific	Cat#35050061
LPS Salmonella minnesota R595 - TLR4 ligand	InvioGen	Cat#15C10-MM
bis(sulfosuccinimidyl)suberate, disodium salt (BS3)	FUJIFILM Wako	Cat# B574
Sodium deoxycholate (SDC)	FUJIFILM Wako	Cat#194-08311
Sodium N-lauroylsarcosinate (SLS)	FUJIFILM Wako	Cat#192-10382
Trifluoroacetic acid (TFA)	FUJIFILM Wako	Cat#204-02743
Ammonium acetate	FUJIFILM Wako	Cat#015-02837
Dimethyl sulfoxide (DMSO)	FUJIFILM Wako	Cat#041-29351
Ponceau-S Staining Solution	Beacle	Cat#BCL-PSS-01
100 x protease inhibitor cocktail	Merck	Cat#P8340
Lysyl endopeptidase (LysC)	FUJIFILM Wako	Cat#129-02541
Trypsin	Promega	Cat#V5111
SETAPAETATPAPVEKSPAKK-K(biotin), Ac-SETAPAETATPAPVEKSPAKK-K(biotin), Ac-SETAPAETATPAPVEKpSPAKK-K(biotin)	Synpeptide	N/A

(*Continued on next page*)

Continued

REAGENT or RESOURCE	SOURCE	IDENTIFIER
Nuclease-Free Water (not DEPC-Treated)	Thermo Fisher Scientific	Cat# AM9937
TurboDNase (2U/uL)	Thermo Fisher Scientific	Cat# AM2238
SUPERaseIn	Thermo Fisher Scientific	Cat# AM2694
cOmplete Mini, EDTA-free Protease Inhibitor Cocktail	Sigma-Aldrich	Cat# 11836170001
QIAzol lysis reagent	QIAGEN	Cat# 79306
Trizol LS reagent	Thermo Fisher Scientific	Cat# 10296028
Critical commercial assays		
SuperScript III First-Strand Synthesis SuperMix for qRT-PCR	Thermo Fisher Scientific	Cat# 11752050
TaqMan Gene Expression Master Mix	Thermo Fisher Scientific	Cat# 4369016
Empore SDB-XC membrane	GL Sciences	Cat#5010-30016
Empore cation-SR membrane	GL Sciences	Cat#5010-30031
Dynabeads Protein G Magnetic Beads	Thermo Fisher Scientific	Cat#10003D
Pierce™ High Capacity Streptavidin Agarose	Thermo Fisher Scientific	Cat#20357
ReproSil-Pur C18-AQ materials 120 (3 μm)	Dr. Maisch GmbH, Ammerbuch	Cat#r13.aq.
ECL reagent	Cytiva	Cat#RPN2124
Deposited data		
Proteomic raw data	this paper	jPOST: PXD024078
Proteomic raw data	this paper	jPOST: PXD031475
Proteomic raw data	this paper	jPOST: PXD024080
Proteomic raw data	this paper	jPOST: PXD024081
Proteomic raw data	this paper	jPOST: PXD024104
Proteomic raw data	this paper	jPOST: PXD026349
Experimental models: Cell lines		
Human: HeLa	ATCC	Cat# CCL-2, RRID: CVCL_0030
Mouse: RAW264.7	ATCC	Cat#TIB-71, RRID:CVCL_0493
Oligonucleotides		
RPS27 (Hs01378332_g1) TaqMan Assay	Thermo Fisher Scientific	Cat# 4331182
RPL12 (Hs02385039_g1) TaqMan Assay	Thermo Fisher Scientific	Cat# 4331182
RPL5 (Hs00851991_u1) TaqMan Assay	Thermo Fisher Scientific	Cat# 4331182
RPS17 (Hs00734303_g1) TaqMan Assay	Thermo Fisher Scientific	Cat# 4331182
GammaTub23C (Dm01841764_g1) TaqMan Assay	Thermo Fisher Scientific	Cat# 4331182
Software and algorithms		
MaxQuant (v1.6.17.0 or v.1.6.2.10)	Cox and Mann, 2008	https://www.maxquant.org/
Perseus (v.1.6.5.0)	Tyanova et al., 2016	https://maxquant.net/perseus/
Metascape	Zhou et al., 2019	https://metascape.org/gp/index.html#/main/step1
FAIMS MzXML Generator	Hebert et al., 2018	https://github.com/coongroup/FAIMS-MzXML-Generator
R Studio (v 1.2.5001)	Rstudio team	https://www.rstudio.com/

RESOURCE AVAILABILITY

Lead contact

Further information and requests for resources and reagents should be directed to and will be fulfilled by the Lead Contact, Koshi Imami (koshi.imami@riken.jp).

Materials availability

This study did not generate new unique reagents.

Data and code availability

The proteomics data have been deposited to the ProteomeXchange Consortium via the jPOST (Moriya et al., 2019; Okuda et al., 2017) partner repository with the dataset identifier, PXD024078 (pSNAP evaluation related to Figures 1D and S2A), PXD031475 (LPS experiment related to Figure S2C), PXD024080 (silmitasertib experiment related to Figure 3A), PXD024081 (Nt-acetylation related to Figure 4A), PXD024104 (mouse primary culture related to Figures 2A and 2D, and PXD026349 (peptide pulldown related to Figure 4G). This paper does not report original code. Any additional information required to reanalyze the data reported in this paper is available from the lead contact upon request.

EXPERIMENTAL MODEL AND SUBJECT DETAILS

HeLa cell culture and pulse labeling with puromycin and SILAC amino acids

HeLa cells (ATCC) were cultured in Dulbecco's modified Eagle's medium (DMEM) (FUJIFILM Wako) supplemented with 10% fetal bovine serum (FBS) (Thermo Fisher Scientific). Cells were grown to approximately 70–80% confluence and then used for experiments. For pulse-labeling experiments, the cell culture medium was switched to arginine- and lysine-free DMEM (Thermo Fisher Scientific) supplemented with 10% FBS and 10 μM puromycin (FUJIFILM Wako), either "heavy" amino acids [0.398 mM L-($^{13}C_6$,$^{15}N_4$)-arginine (Arg"10") and 0.798 mM L-($^{13}C_6$,$^{15}N_2$)-lysine (Lys"8")] or "medium" amino acids [0.398 mM L-($^{15}N_4$)-arginine (Arg"4") and 0.798 mM L-(D_4)-lysine (Lys"4")] (Cambridge Isotope Laboratories), and incubated for 30 min or 2 h as described elsewhere (Imami et al., 2010, 2018; Uchiyama et al., 2020). For the proof-of-concept experiment (related to Figure 1B), HeLa cells were pulse-labeled with a combination of 10 μM puromycin and 'heavy' amino acids (Arg'10' and Lys'8') for 2 h, while as control, cells were treated with only 'medium-heavy' amino acids (Arg'4' and Lys'4') and puromycin was omitted. To examine the degradation of puromycylated NPCs during puromycin labeling (related to Figure S1B), HeLa cells were treated with 10 μM puromycin and either DMSO, 10 μM MG-132 (Chemscene) or 1 μM bortezomib (FUJIFILM Wako) for 15 min, 30 min, 60 min, and 120 min. In the silmitasertib experiment (related to Figure 3A), HeLa cells were pre-incubated with either DMSO or a CK2 inhibitor silmitasertib (MedChemExpress) (10 μM) for 10 min, and then pulse-labeled with puromycin for 2 h in the presence of either DMSO (+'medium-heavy' amino acids) or 10 μM silmitasertib (+'heavy' amino acids). For the protein Nt-acetylation profiling (related to Figure 4A), HeLa cells were pulse-labeled with puromycin for 2 h in the presence of either 100 μg/mL CHX (FUJIFILM Wako) (+'medium-heavy' amino acids) or DMSO (+'heavy' amino acids). After pulse-labeling, cells were washed twice with ice-cold PBS and collected by centrifugation. Three independent experiments were performed in all proteomic studies. All cells were maintained in an incubator at 37°C under humidified 5% CO_2 in air.

Mouse primary cortex cultures and pulse labeling

Primary cultures of cortical neurons were prepared as described with a few modifications (Kaech and Banker, 2006). In brief, cortices were dissected from postnatal day 0 (P0) mice. Cortical neurons were dissociated using neuron dissociation solutions (FUJIFILM Wako) and plated on 35 mm (DIV7 neuron pulse labeling) or 60 mm (DIV5 and DIV14 neuron pulse labelling) dishes coated with poly-L-lysine (Merck) at a density of 1×10^5 and 2×10^5 cells/cm^2, respectively, in MEM (Thermo Fisher Scientific) supplemented with 10% horse serum (Thermo Fisher Scientific), 0.6% D-glucose (Merck), 1 mM sodium pyruvate (Nacalai Tesque) and 1% penicillin-streptomycin (Thermo Fisher Scientific). Three hours after plating, the media was replaced by growth media consisting of Neurobasal-A medium (Thermo Fisher Scientific) supplemented with B-27 supplement (Thermo Fisher Scientific), GlutaMAX (Thermo Fisher Scientific) and penicillin-streptomycin (Thermo Fisher Scientific). Neurons were maintained at 37°C in 5% CO_2 until experiments. For pulse labeling experiments at 7 days *in vitro* (related to Figure 2A) and experiments to assess differential translations between 5 and 14 days *in vitro* (related to Figure 2D), the cell culture medium was switched to arginine- and lysine-free Neurobasal-A medium (Research Institute for the Functional Peptides) supplemented with B-27 supplement, GlutaMAX, penicillin-streptomycin and either "heavy" amino acids or "medium-heavy" amino acids, and processed as described above. ICR mice were purchased (Shimizu). This study was carried out in accordance with the Guide for the Care and Use of Laboratory Animals from the Society for Neuroscience and was authorized by the Animal Care and Use Committee of Kyoto University.

RAW264.7 cell culture and pulse labeling

RAW264.7 cells (ATCC) were cultured in DMEM supplemented with 10% FBS. For lipopolysaccharide (LPS) stimulation experiments (related to Figure S2C), cells were grown to approximately 70% confluence and then used for experiments. Cells were pre-incubated with either 100 ng/mL LPS [Salmonella minnesota R595 - TLR4 ligand (InvivoGen 15C10-MM)] or vehicle (ultrapure water) for 1 h, and then pulse-labeled with puromycin for 30 min, 1 h or 2 h in the presence of either 'medium-heavy' amino acids (for control cells) or 'heavy' amino acids (for LPS-stimulated cells). Three independent experiments were performed for each condition. Cells were maintained in an incubator at 37°C under humidified 5% CO_2 in air.

METHOD DETAILS

Immunoprecipitation (IP) of NPCs with anti-puromycin antibody

HeLa cell pellets were lysed with a buffer [100 mM HEPES-NaOH (pH 7.5), 150 mM NaCl, 1% Nonidet P-40 (NP-40), protease inhibitor cocktail (Merck)], and cell debris was removed by centrifugation (4°C, 16,000 x g, 30 min). Mouse primary cells were washed twice with ice-cold PBS and directly lysed by using lysis buffer [100 mM HEPES-NaOH (pH 7.5), 150 mM NaCl, 1% Nonidet P-40 (NP-40), 1% protease inhibitor cocktail (Merck)] and further centrifuged at 21,500 x g for 5 min at 4°C to remove cell debris. The protein concentration was measured using a BCA assay (Thermo Fisher Scientific), and 250 μg (1 μg/μL) protein per sample was used for the following IP, except that 250, 500, or 750 μg protein was used for the experiment with 30 min pulse labeling (related to Figure S2A) and that 140, 280, and 560 μg protein were used for 2 h, 1 h, and 30 min pulse labeling in the LPS treatment experiments (related to Figure S2C). For the silmitasertib treatment experiments (related to Figures 3A), 125 μg protein inputs from 'medium-heavy'- and 'heavy'-labeled cells were combined (total 250 μg proteins). 62.6 μg Dynabeads™ Protein G Magnetic Beads (Thermo Fisher Scientific) and 15 μg anti-puromycin antibody (clone 12D10 from Merck Millipore or 3RH11 from Cosmo Bio) per IP experiment were mixed in PBS-0.02% Tween 20 (PBS-T) and incubated for 30 min at room temperature with rotation. The supernatant was removed and the beads were washed twice with a conjugation buffer (PBS). To crosslink the beads and the antibodies, the beads were suspended in 5 mM bis(sulfosuccinimidyl)suberate, disodium salt (BS^3, Wako FUJIFILM) in the conjugation buffer and incubated for 30 min at 37°C. To quench the reaction, 50 mM (final concentration) Tris-HCl pH 7.5 was added and incubation was continued for 15 min at room temperature. The antibody-conjugated beads were then rinsed with 0.02% PBS-T, PBS, and the lysis buffer. The antibody-conjugated beads were incubated with 250 μg protein input for 1 h at 4°C with slow rotation. The supernatant was transferred to a new tube, and the beads were washed three times with PBS supplemented with 850 mM NaCl. Puromycylated NPCs were eluted from the beads with 100 μL 0.15% trifluoroacetic acid (TFA) (FUJIFILM Wako), and the elution was repeated once more. All TFA eluates were combined and dried in a SpeedVac (Thermo Fisher Scientific).

Protein digestion and SCX fractionation

The dried samples were resuspended with 100 mM Tris-HCl pH 9.0 containing 8 M urea. Proteins were reduced with 10 mM dithiothreitol (DTT) (FUJIFILM Wako) for 30 min at 37°C, followed by alkylation with 50 mM 2-iodoacetamide (IAA) (FUJIFILM Wako) for 30 min at room temperature in the dark. The samples were diluted to 2 M urea with 50 mM ammonium bicarbonate. The proteins were digested with 1 μg lysyl endopeptidase (LysC) (FUJIFILM Wako) and 1 μg trypsin (Promega) overnight at 37°C on a shaking incubator. The resulting peptides were acidified with 0.5% TFA (final concentration), and fractionated with a StageTip containing SDB-XC (upper) and SCX (bottom) Empore disk membranes (GL Sciences) (Adachi et al., 2016). Peptides were eluted from the tip sequentially using 1) 0.5% TFA and 30% acetonitrile (ACN) 2) 1% TFA and 30% ACN 3) 2% TFA and 30% ACN, 4) 3% TFA and 30% ACN 5) 3% TFA, 100 mM ammonium acetate and 30% ACN 6) 4% TFA, 500 mM ammonium acetate and 30% ACN, and 7) 500 mM ammonium acetate and 30% ACN (related to Figures 1B, 2A, and 3A). For protein Nt-acetylated profiling (related to Figure 4A), flowthrough and wash (with 0.1% TFA and 80% ACN) fractions, in which Nt-acetylated peptides are expected to be enriched were combined and measured by LC/MS/MS. The sample solution was evaporated in a SpeedVac and the residue was resuspended in 0.5% TFA and 4% ACN. For the experiments related to Figures 2D, S2A, S2C, and 4G, the digested peptides were desalted using SDB-XC StageTips prior to LC/MS/MS analysis (no SCX fractionation was performed).

Peptide pulldown assay

Synthetic peptides were purchased from Synpeptide, and peptide sequences used were as follows: SETAPAETATPAPVEKSPAKK-K(biotin), Ac-SETAPAETATPAPVEKSPAKK-K(biotin), and Ac-SETAPAETA

TPAPVEKpSPAKK-K(biotin). Synthetic peptides (60 nmol each) were incubated with 18 μL streptavidin agarose resins (high-capacity streptavidin agarose, Thermo Fisher Scientific) per experiment for 2 h at room temperature in 80 μL of lysis buffer (1% NP-40, 150 mM NaCl, 25 mM Tris-HCl pH 7.5, and protease and phosphatase inhibitor cocktails). Synthetic peptides bound to agarose resins were incubated with HeLa cell lysate (300 μg in 500 uL lysis buffer) for 2 h at 4°C. Resins were washed three times with 1 mL of lysis buffer, and proteins bound to resins were eluted with 60 μL of elution buffer [12 mM sodium deoxycholate, 12 mM sodium N-lauroylsarcosinate, 5 mM DTT, 100 mM Tris-HCl pH 9.0]. Afterward, samples were transferred to new tubes and processed for LC/MS/MS analysis as described elsewhere (Masuda et al., 2008) Figure 4F.

Mass spectrometry and data acquisition

Nano-scale reversed-phase liquid chromatography coupled with tandem mass spectrometry (nanoLC/MS/MS) was performed by an Orbitrap Fusion Lumos mass spectrometer (Thermo Fisher Scientific) connected to a Thermo Ultimate 3000 RSLCnano pump and an HTC-PAL autosampler (CTC Analytics, Zwingen, Switzerland) equipped with a self-pulled analytical column (150 mm length × 100 μm i.d.) (Ishihama et al., 2002) packed with ReproSil-Pur C18-AQ materials (3 μm, Dr. Maisch GmbH, Ammerbuch, Germany). The mobile phases consisted of (A) 0.5% acetic acid and (B) 0.5% acetic acid and 80% ACN. Peptides were eluted from the analytical column at a flow rate of 500 nL/min with the following gradient: 5–10% B in 5 min, 10–40% B in 60 min, 40–99% B in 5 min, and 99% for 5 min.

For most of the experiments (related to Figures 1B, 2A, 3A, and 4A), the Orbitrap Fusion Lumos instrument was operated in the data-dependent mode with a full scan in the Orbitrap followed by MS/MS scans for 3 s using higher-energy collisional dissociation (HCD). The applied voltage for ionization was 2.4 kV. The full scans were performed with a resolution of 120,000, a target value of 4×10^5 ions, and a maximum injection time of 50 ms. The MS scan range was *m/z* 300–1,500. The MS/MS scans were performed with a 15,000 resolution, a 5×10^4 target value, and a 50 ms maximum injection time. The isolation window was set to 1.6, and the normalized HCD collision energy was 30. Dynamic exclusion was applied for 20 s. For the nascent proteome analyses of mouse primary cultures (Figure 2D) and RAW264.7 cells treated with LPS (Figure S2C), and the peptide pulldown assay (Figure 4F), the mass spectrometric analyses were carried out with the FAIMS Pro interface (Thermo Fisher Scientific). The compensation voltage (CV) was set to −40, −60, and −80, and the cycle time of each CV experiment was set to 1 s. The full scans were performed with a resolution of 120,000, the standard AGC target mode, and a maximum injection time of 50 ms. The MS scan range was *m/z* 300–1,500. The MS/MS scans were collected in the ion trap with the rapid mode, the standard AGC target mode, and a maximum injection time of 30 ms. The isolation window was set to 1.6, and the normalized HCD collision energy was 30. Dynamic exclusion was applied for 20 s.

For the nascent proteome analyses with short pulse labeling (related to Figure S2A), the LC/MS/MS analyses were performed on an UltiMate 3000 RSLCnano system (Thermo Fisher Scientific), combined with an Orbitrap Exploris 480 mass spectrometer (Thermo Fisher Scientific). All mass spectrometric analyses were carried out in the data-dependent acquisition (DDA) mode. For the Orbitrap Exploris 480 system, peptides were separated on self-pulled needle columns (250 mm, 100 μm ID) packed with Reprosil-Pur 120 C18-AQ1.9 μm (Dr. Maisch, Ammerbuch, Germany) at 50°C in a column oven (Sonation). The flow rate was 400 nL/min. The flow gradient was set as follows: 5% B in 5 min, 5–19% B in 55.3 min, 19–29% B in 21 min, 29–40% B in 8.7 min, and 40–99% B in 0.1 min, followed by 99% B for 4.9 min. The electrospray voltage was set to 2.4 kV in the positive mode. The mass spectrometric analysis was carried out with the FAIMS Pro interface. The FAIMS mode was set to a standard resolution, and the total carrier gas flow was 4.0 L/min. The CV was set to −40 and −60, and the cycle time of each CV experiment was set to 1 s. The mass range of the survey scan was from 375 to 1,500 m/z with a resolution of 60,000, 300% normalized automatic gain control (AGC) target and auto maximum injection time. The first mass of the MS/MS scan was set to 120 m/z with a resolution of 15,000, standard AGC, and auto maximum injection time. Fragmentation was performed by HCD with a normalized collision energy of 30%. The dynamic exclusion time was set to 20 s.

Processing of mass spectrometry data

All raw data files were analyzed and processed by MaxQuant (Cox and Mann, 2008) (v1.6.17.0 or v.1.6.2.10), and the database search was performed with Andromeda(Cox et al., 2011) against the SwissProt database (version 2020-10, 42,372 human protein entries) or mouse UniProt database (version 2020-3, 55,462 protein

entries) spiked with common contaminants and enzyme sequences. Raw data files collected from FAIMS experiments were split into a set of MaxQuant compliant MzXML files using FAIMS MzXML Generator (https://github.com/coongroup/FAIMS-MzXML-Generator) (Hebert et al., 2018). Search parameters included two missed cleavage sites and variable modifications such as L-($^{13}C_6$,$^{15}N_4$)-arginine (Arg10 = heavy Arg, +10.00827), L-($^{13}C_6$,$^{15}N_2$)-lysine (Lys8 = heavy Lys, +8.01420), L-($^{15}N_4$)-arginine (Arg 4 = medium-heavy Arg, +3.98814 Da), L-(D_4)-lysine (Lys 4 = medium-heavy Lys, +4.02511), methionine oxidation, protein N-terminal acetylation and phosphorylation of tyrosine, serine and threonine (only for the silmitasertib experiment related to Figure 3A and Nt-acetylome experiment related to Figure 4A). Cysteine carbamidomethylation was set as a fixed modification. The peptide mass tolerance was 4.5 ppm, and the MS/MS tolerance was 20 ppm. The false discovery rate (FDR) was set to 1% at the peptide spectrum match (PSM) level and protein level.

For protein-level quantification in all experiments, 'unique + razor' peptides were used. For the SILAC-based protein quantification, a minimum of one ratio count (unique peptide ion) was used for quantification, and the 're-quantify' and 'match between runs' functions were employed. Raw H/M ratios were used for quantification related to Figures 1A, 2A, 4A, and S2A while normalized H/M ratios were used for the differential analysis of NPC levels (related to Figures 2D, 3A, and S2C). For label-free quantification of peptide pulldown samples (related to Figure 4F), a minimum of two ratio counts was used for quantification. Only proteins quantified in 2 out of the 3 replicates in at least one condition were used for further analysis, and missing values were imputed from a normal distribution of $\log_2$ LFQ intensity using a default setting (width 0.3, down shift 1.8) in Perseus (v.1.6.5.0) (Tyanova et al., 2016). Volcano plots were generated based on $\log_2$ FC (x-axis) and -$\log_{10}$ p-value from two-sided *t*-test (y-axis). The curve indicates a cut-off for differentially interacting proteins (FDR<0.05, s0: 0.8).

For the differential NPC analysis in mouse primary cortex cultures (related to Figure 2D), normalized H/M ratios were $\log_2$ transformed and replicates were averaged when they were quantified in at least two of the three replicates. Two-sided one sample *t*-tests were performed on the experimental data using Perseus (Tyanova et al., 2016) and proteins were considered as 'significantly regulated' when they were below a *t*-test p-value of 0.05 and above 0.5 (a $\log_2$ ratio) according to an FDR estimation of SILAC fold-change (Bogdanow et al., 2020). To do this, we used the simulated data as a false positive set and accepted proteins above a SILAC fold-change that recalled <5% false positives. Our criteria (p-value of 0.05 and above 0.5 (a $\log_2$ ratio)) correspond to FDR<0.05.GO enrichment (Figure 2G) of the significantly regulated proteins were performed using Metascape (Zhou et al., 2019).

For phosphosite analysis (related to Figure 3D), only class I (localization probability>0.75) sites (Olsen et al., 2006) that were quantified in at least one of the replicates were used.

Analysis of the positions of identified peptides within protein sequences

To calculate the positions of identified peptides within protein sequences (related to Figures 1E, 2C, S2B, S3A, and S4B), we classified peptides into two groups based on their H/M ratios; H/M≧2 (i.e., NPCs) and H/M < 2 (i.e., potential contaminants). The first amino acids within peptides were mapped onto a protein sequence, and their relative positions within proteins (from N-term: 0 to C-term: 1) were calculated. For the input samples, all identified peptides were used to compute the positions within proteins. Only M− and H-labeled peptides were considered to calculate the positions within protein sequences in Figure S3A.

Comparison of pSNAP with pSILAC and ribo-seq

To compare the three orthogonal approaches (pSNAP, pSILAC, and ribo-seq) (related to Figure SX), we used intensity-based absolute quantification (iBAQ) intensities (Schwanhäusser et al., 2011) from proteomic analysis and read counts of ribosome protected fragments (RPFs) obtained from ribo-seq. The iBAQ algorithm computes the sum of all peptides intensities divided by the number of theoretically observable peptides, which provides a rough estimation of protein abundance within a sample. In pSNAP and pSILAC experiments (Figure 1E), iBAQ intensities from the 'heavy' channel were used as a relative protein abundance of nascent proteins within the sample and compared to the read counts of RPFs obtained from the ribo-seq. The pSILAC data was obtained from the input sample (Figure 1E: without enrichment of NPCs) in which 2 h pulse labeling was performed. Ribo-seq data were obtained from a previously published dataset (Stumpf et al., 2013) in which cell cycle-dependent (i.e., G1, S, M) translational changes were analysed in HeLa cells. Transcripts having read counts within 0–10 were eliminated. For our pSNAP result, we

only used proteins showing H/M ratio >2 as those proteins are more likely to be *bona fide* NPCs. To compare our proteomic result (asynchronous HeLa cells) with the ribosome profiling data, we used data from the G1 cell-cycle stage because G1 is the major cell-cycle phase in asynchronous cells.

Western blotting

The cell lysates were re-suspended in LiDS loading sample buffer (Thermo Fisher Scientific) with 50 mM DTT and incubated at 70°C for 5 min. The protein samples were loaded onto a 4–12% gradient SDS-polyacrylamide gel (Thermo Fisher Scientific) and separated using electrophoresis. The proteins were then transferred to a PVDF membrane (Merck Millipore) using a semi-dry western blot transfer system set to a constant current of 200 mA for 30 min. The membranes were first blocked by incubation in 5% (w/v) BSA or 5% (w/v) skim milk in Tris-buffered saline and 0.1% tween 20 (TBS-T) and then incubated with anti-puromycin antibody (clone 3RH11, Cosmo Bio) diluted 1:5,000, overnight at room temperature. The membrane was washed three times with 0.1% TBS-T, incubated with HRP-conjugated anti-mouse secondary antibody (1: 20,000 dilution) in 0.1% TBS-T 1 h at room temperature, washed three times in TBS-T, and developed with ECL reagent (Cytiva). Ubiquitinated proteins were detected using anti-ubiquitin rabbit antibody (CST) (1: 2,000 dilution) and HRP-conjugated anti-rabbit secondary antibody (1: 10,000 dilution). Chemiluminescence was detected using the luminescent image analyzer ImageQuant LAS-500 (Cytiva).

qRT-PCR analysis of selected transcripts in monosome and polysome fractions

HeLa cells (70% confluence) were treated with either 10 μM silmitasertib or DMSO for 2 h. Two independent experiments were performed. The cells were placed on ice and gently washed once with 10 mL ice-cold PBS. Then they were lysed with 0.4 mL ice-cold lysis buffer (20 mM Tris-HCl, pH 7.5, 150 mM NaCl, 5 mM $MgCl_2$, 1 mM DTT, Complete EDTA-free Protease Inhibitor Cocktail, 100 μg/mL cycloheximide, 1% Triton X-100, 25 units/mL Turbo DNase (Thermo Fisher Scientific), and 100 units/mL SUPERaseIn (Thermo Fisher Scientific)). The lysate was incubated on ice for 10 min and triturated through a 25-gauge needle (Terumo) ten times before centrifugation at 20,000 x g for 10 min at 4°C. The supernatant was collected in a new tube for the sucrose gradient analysis and as the sample for loading. A 10–45% continuous sucrose gradient was prepared in a polyclear tube (Seton) using 10 and 45% sucrose buffers containing 100 μg/mL cycloheximide and 1 mM DTT in polysome buffer (25 mM Tris-HCl (pH 7.5), 150 mM NaCl and 15 mM $MgCl_2$) and the Biocomp Gradient Master program (Biocomp). An equal amount of cell lysate to the sample (300 μL) was loaded on the prepared gradient solution. Monosome and polysomes were separated in the sucrose gradient by ultracentrifugation using a SW-41 rotor (Beckman Coulter) at 36,000 rpm for 2.5 h at 4°C.The profile of relative RNA abundances of monosomes and polysomes were visualized at 254-nm wavelength, and equal-volume fractions were collected simultaneously with the Biocomp Piston Gradient Fractionator (Biocomp) Figure 3C.

For the RNA analysis, an equal sample volume of TRIzol LS reagent (Thermo Fisher Scientific) was immediately added to the fractions and loading sample. RNA was purified using an miRNeasy Mini Kit according to manufacturer's instructions. Purified RNAs along with 1 ng of spiked *Drosophila* RNA were used for single strand complementary DNA (cDNA) synthesis using a SuperScript III First-Strand Synthesis SuperMix for qRT-PCR (Thermo Fisher Scientific). Quantitative RT-PCR was performed using TaqMan Gene Expression Master Mix (Thermo Fisher Scientific) on a Quant Studio 3 instrument (Thermo Fisher Scientific). The cDNA synthesis rate is validated by the spiked *Drosophila* RNA and the sample Ct values were compared with the loading sample before the sucrose gradient.

QUANTIFICATION AND STATISTICAL ANALYSIS

The type of statistical test (e.g., Wilcoxon rank-sum) is annotated in the Figure legend and/or in the Methods specific to the analysis. In addition, statistical parameters such as the value of n, mean/median, SD and significance level are reported in the Figures and/or in the Figure Legends. Statistical analyses were performed using R as described in Methods and Resources for each individual analysis.